Experiments in Fluids 24 (1998) 238–245 © Springer-Verlag 1998

Shape of a shock wave front diffracting on a perforated wall

H. Onodera

Abstract The shape of a shock wave front diffracting on a perforated wall is determined by comparing numerical data and experimental findings. Experiments were conducted in a 60 mm × 150 mm cross sectional area shock tube equipped with a double-exposure holographic interferometer. The numerical simulation was conducted using a TVD upwind finite difference scheme. First, a discharge coefficient for the mass flow through the perforations was determined by comparing the numerical results with those obtained using a simplified quasi-one-dimensional analysis. This value agreed well with the experimentally obtained value. Finally, the shape of a backward inclined incident shock wave over a perforated wall was successfully determined by employing this discharge coefficient and the numerical result.

List of symbols

A	two-dimensional perforated area
a	speed of sound
L	distance between the first slit and the shock front
(m)	mass flux
Ms	incident shock wave Mach number
P	intersection point of the incident shock wave and the perforated wall
s	interval between slits
t	time
u	component of the flow velocity in the x-direction
v	component of the flow velocity in the y-direction
x	x-direction
y	y-direction
Δx	interval of one computational mesh in the x-direction
Δy	interval of one computational mesh in the y-direction
γ	specific heats ratio
ε	perforation ratio
ζ	flow discharge coefficient
ρ	density
χ	glancing incidence angle

Indices

0	initial condition
2	flow condition behind the incident shock wave
4	flow condition inside the perforation
qs	quasi-one-dimensional analysis
re	reservoir condition
st	stagnation condition
max	maximum value obtained in numerical simulation

Received: *17 March 1995*/*Accepted*: *13 August 1997*

H. Onodera
Center for Cooperative Research and Development
Iwate University, Ueda, Morioka, Iwate 020, Japan

The author would like to express his gratitude to Professor K. Takayama of the Shock Wave Research Center, Tohoku University, Japan and Professor O. Igra of the Ben-Gurion University of the Negev, Israel, for their discussions on this paper. The author is also indebted to Dr. O. Onodera and Mr. H. Ojima of the Institute of Fluid Science, Tohoku University, for their assistance in conducting the present experiments. The author acknowledge with thanks the help of Mr. S. Hayasaka of the machine shop of the institute of Fluid Science, Tohoku University, for his manufacturing of the present shock tube and models.

1 Introduction

It is reported that noise or vibration which appears in pneumatic machines or pipe line systems are caused by shock waves propagation (Okutsu 1984), or are due to shock wave emerging from the pipe open end. The emerging shock wave, even when it is weak, may cause a noise problem similar to a sonic boom. Similar phenomena are found in automobile engines. Weak shock waves generated in exhaust manifolds of internal combustion engines cause a metallic noise from the silencers (Matsumura and Onodera 1991). In the case of railway systems, compression waves generated by a high speed train entering a tunnel can coalesce into a shock wave and create a boom at the tunnel exit (Aoki et al. 1991; Kage et al. 1992).

From an industrial point of view, it is important to understand the movement of shock waves in pipe line systems. Once this is understood, the noise induced in the pipe line systems, or shock induced vibrations, could be controlled.

It has been reported that porous materials are effective in attenuating shock waves and, therefore, shock wave propagation in porous media or along a perforated wall has been the subject of many studies, e.g., Szumowski (1971); Lee et al. (1976); Frolov and Gelfand (1991). Shock wave propagation over a perforated wall is a complicated phenomenon and therefore, it is difficult to clearly identify the details of the flow mechanism responsible for attenuating the shock wave and thereby regulating the flow behind it.

As a first attempt a quasi-one-dimensional flow model was used. The attenuation of a shock wave propagating in a

perforated pipe was analyzed and subsequently, the discharge coefficient (defined as the ratio between the real discharge and the theoretically predicted value) was empirically obtained (Szumowski 1971; Deckker and Koyama 1983). This discharge coefficient was employed as a parameter for fitting the quasi-one-dimensional results to experimentally obtained data. However, in reality shock wave propagation and the flow field induced in a perforated pipe are not one-dimensional. Therefore, the predictions based on a quasi-one-dimensional model show discrepancies when compared with experimental results.

For predicting the shape of a shock wave diffracting around a corner, the CCW (Chester, Chisnell and Whitham) theory, suggested by Whitham (1957), is employed. However, the shape of a diffracting shock wave predicted by the CCW theory, does not agree with experimental findings. De Bore (1963) analyzed the local curvature of shock fronts disturbed by the wall boundary layer developed in a shock tube. He employed the small perturbation theory assuming that the shock front, on the side wall, is disturbed due to a local change in the wall curvature caused by the side wall boundary layer displacement thickness. However, to the best of author's knowledge, there is no applicable method to predict the shape of a shock wave diffracting over a perforated wall.

The shape of a diffracting shock wave is controlled by the mass outflow velocity from perforations and by the main flow velocity. Therefore, when using the simple quasi-one-dimensional analysis it is necessary to employ an adequate discharge coefficient. By using an appropriate discharge coefficient, one can obtain mass outflow velocity through perforations from analysis.

In the present paper, a TVD scheme is employed for describing the two-dimentional flow field developed behind a diffracting shock wave. In addition, a physically reliable discharge coefficient (Onodera and Takayama 1994), which was obtained from quantitative comparison between numerical results and quasi-one-dimensional analysis, is used for determining the shape of the diffracting shock wave front.

2
Experimental facility

Experiments were conducted in a 60 mm × 150 mm shock tube of the Shock Wave Research Center, Institute of Fluid Science, Tohoku University. A detailed discription of this facility is available in Onodera and Takayama (1990a).

Mylar diaphragms of 100, 188 and 250 μm thickness were used. The test gas was air ($\gamma = 1.4$) at initial pressures within the range from 60 to 100 kPa, and for driver gases, nitrogen or helium were used. Incident shock wave Mach numbers (Ms) thus obtained were 1.54, 1.85 and 2.17, respectively. The scatter in the shock wave Mach numbers was less than $\pm 1\%$. The perforated wall was made of a 60 mm wide and 110 mm long steel plate on which 36 slits of 1 mm width and 7 mm deep were machined at 2.5 mm intervals. The perforation ratio, i.e. the ratio of the rigid wall area to the perforated area, was 0.4.

For flow visualization, a double exposure holographic interferometer was used. A Q-switched ruby laser (Apollo Lasers Inc., 22HD, 694.3 nm wave length, 2 J/pulse and 25 ns pulse duration) was used as a light source. The laser was triggered by an output signal from a pressure transducer through a delay unit (Sugawara RE-306). The velocity of the incident shock wave was measured using two pressure transducers (Kistler 606L) placed 250 mm apart, just ahead of the shock tube test section.

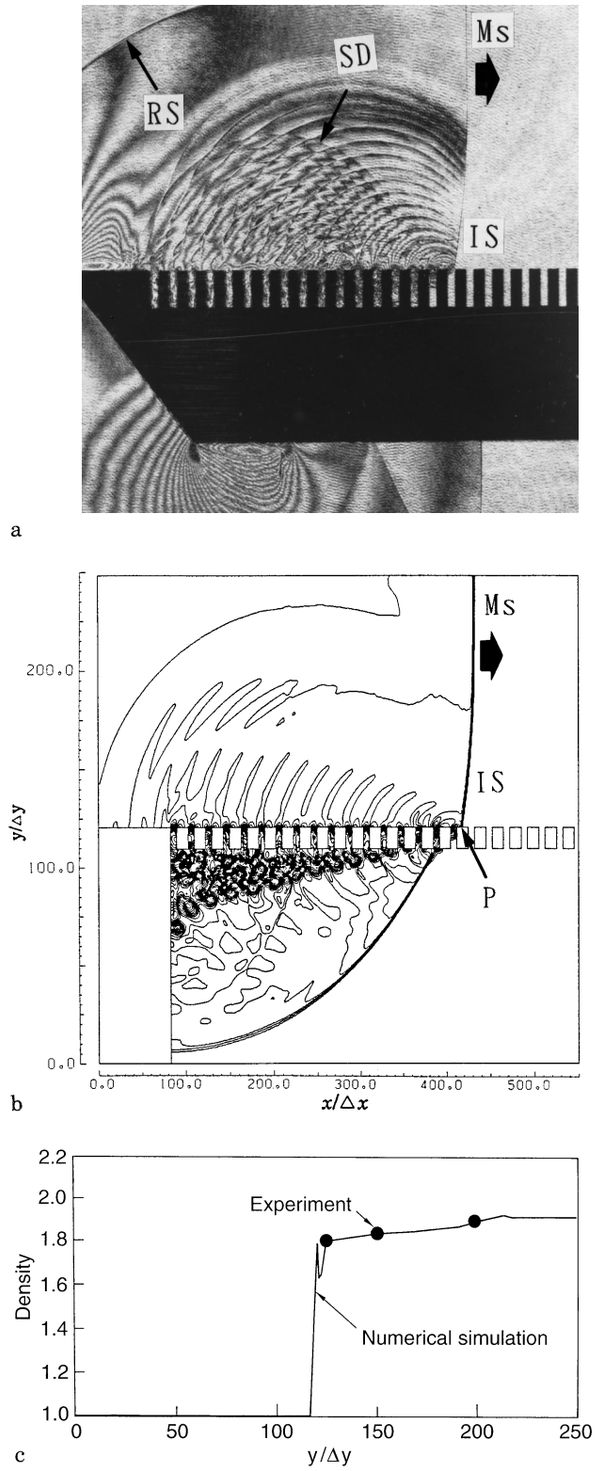

Fig. 1a–c. Comparison between experimental and numerical simulation. **a** Interferogram; **b** numerical simulation; **c** density distribution behind the incident shock wave

3
Numerical simulation

For simulating the shock wave propagation over the perforated wall, a TVD finite difference scheme (Yee 1989) was used in solving the two-dimensional unsteady Euler equations. The boundary conditions for the computational domain (shown in Fig. 1b) are: on the solid boundary, a slip condition is used while at the center line (the top of Fig. 1b), a free boundary condition is employed. The same type of boundary conditions is applied to all solid walls at the slitted region. At the solid wall surfaces, mirror conditions are imposed on the flow velocity component perpendicular to the wall, and slip conditions are used for the flow velocity component parallel to the wall. At the entrance to the computational domain, conditions given by the Rankine–Hugoniot shock relation for the given *Ms* were imposed. Nine grids were allocated for each of the solid surfaces and six for the perforation in the slitted region. A rectangular grid was used for the present computations, and the entire flow field was covered by 551×251 grid points. Computations were conducted using the super-computer (NEC SX-2N) of the Computer Center of Tohoku University.

4
Determination of the discharge coefficient

As will be shown in Sect. 5, the incident shock wave shape is simulated numerically and compared with experimental findings. It is curved due to its interaction with the perforated wall. For the numerical evaluation of its shape it is necessary to know the value of the discharge coefficient through perforations, and the way in which this is done is described subsequently.

Figure 1a shows an interferogram taken 94 μs after the incident shock wave has reached the first slit. A numerical simulation of this case, showing isopycnics, is given in Fig. 1b. In two-dimensional flows, interferometric fringes correspond to numerically obtained isopycnics; therefore, experimental isopycnics can be compared directly with numerically evaluated isopycnics. The density difference between neighboring computational isopycnics is set to be identical to that observed in the interferogram.

Shock wave diffraction at the entrance to the perforation, shock wave transmission into the perforation, and shock reflection from the perforations bottom can be seen in Fig. 1a. The reflected waves finally emerge into the flow induced behind the incident shock wave and generate secondary disturbances (SD) (Onodera and Takayama 1990a). Unlike the experimental arrangement, in the numerical simulation shown in Fig. 1b, perforations penetrate through the plates thus resulting in flow through the perforations. Therefore, it is reasonable to compare numerically obtained results (Fig. 1b) with predictions based on the quasi-one-dimensional flow assumption. In both cases there is flow through the perforations. For more details, see Onodera and Takayama (1990a, b).

Due to the numerical simulation shown in Fig. 1b, the flow passes through the perforations, and there are no shock reflections, only transmitted waves. In such a case no secondary disturbances exist. It should be noted that when studying the shape of the incident shock wave, while it propagates over a perforated wall, a comparison between experimental results (Fig. 1a) and the numerical simulation shown in Fig. 1b is justified. This is so since, as can be seen from Fig. 1a, the secondary disturbance does not reach the incident shock wave front. At a later time, the secondary disturbance may catch-up with the incident shock wave front. But these reflected secondary shock waves are weakened due to their interaction with the expansion waves emanating from the upstream facing corner of each perforation. The differences in visualized and computed curvature of the incident shock wave are therefore not more than 1% (Onodera 1991). Using these arguments it is allowed to compare the experimental and numerical results, although the perforation geometry in the two cases is somewhat different.

In both Figs. 1a and b, the isopycnic distribution, the shape of the diffracting incident shock front (which is inclined backward due to the presence of expansion waves from the perforations), reflected shock waves from the perforation edges, and vortices are clearly visible. It is also apparent that the experimental and computed flow patterns agree reasonably well with each other. Figure 1c shows the density distribution in the *y*-direction, just behind the incident shock wave. Numerical results agree well with interferometrically obtained data. The proposed physical model and its numerical solution presented here are obviously effective in predicting the considered flow field.

Figure 2 shows the nondimensionalized pressure distribution in the considered flow field 154 μs after the incident shock wave reached the first slit. While the incident shock wave travels along the perforated wall, the region of reduced pressure expands owing to expansion waves emanating from the slits. It is apparent from these results that the maximum pressure ratio obtained behind the incident shock wave is about 2.7. The pressure level in the region extending behind the incident shock wave and the transmitted wave is no longer the same; it substantially drops to about 0.8 at regions inside the perforation zone. The gas flowing around and into the slit is not fully expanded inside each slit, not as assumed in the quasi-one-dimensional analysis; therefore, the pressure behind the transmitted shock wave is not uniform. This is one of the reasons for the discrepancy found between the results obtained while using the quasi-one-dimensional analysis and experimental findings.

In a previous study (e.g. Szumowski 1971), the reservoir condition behind the incident shock wave was kept at the stagnation condition, $P_{re} \equiv P_{st}$; i.e., $P_{re}/P_0 = 3.42$ for $Ms = 1.54$; where P_0, P_{re} and P_{st} denote the initial pressure, reservoir condition, and stagnation condition behind the incident shock wave, respectively. However, the present numerical results suggest that the pressure jump across the incident shock wave is at most 2.7. This means that the effective reservoir pressure, which forces the flow through the slits, is almost the same as the static pressure jump across the incident shock wave, which is 2.6 for $Ms = 1.54$. The reason for this slight discrepancy between the pressure ratio of 2.7 and 2.6 is the interaction of the incident shock wave with the perforations which results in a shock reflection close to the perforation corners and a two-dimensional flow in that region.

It is evident from the above argument that the effective reservoir pressure was overestimated in the former studies. It is reasonable to use the static pressure i.e., 2.6 for $Ms = 1.54$ as the effective reservoir pressure, and not the stagnation pressure of 3.42.

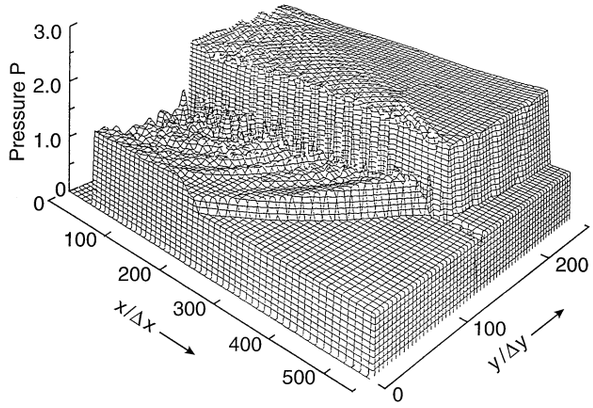

Fig. 2. Pressure distribution in the flow domain (154 μs)

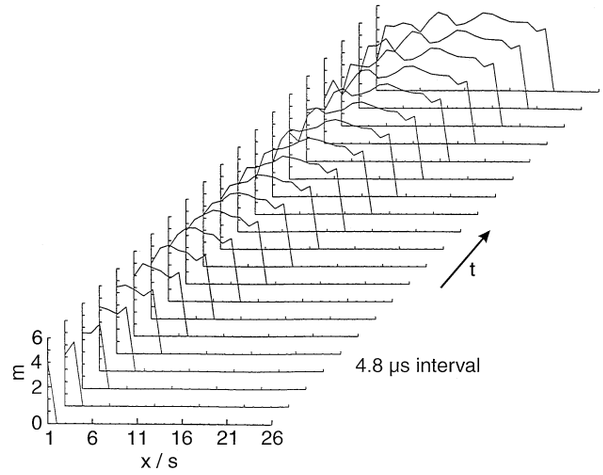

Fig. 3. Outflow mass flux from perforations

The nondimensional mass flux distribution from the perforations computed for a time of 154 μs after the incident shock wave reached the first slit is shown in Fig. 3. When the reservoir conditions exceed the critical pressure ratio of 1.89, the nondimensional mass flux (m) is given by

$$(m) = \rho_0 a_0 A\,(2/(\gamma+1))^{(\gamma+1)/2(\gamma-1)} \tag{1}$$

where A denotes the perforated area. In Eq. (1) the density ρ_0, speed of sound a_0, and the perforation area A were nondimensionalized by ρ_∞, a_∞ and A_∞; A_∞ is the 2-D cell area, i.e., the space between two neighboring grid points, respectively. When taking the numerical value for representing the actual flux, then the flow discharge coefficient is determined as the ratio between the numerically obtained maximum mass flux, i.e., $(m)_{\max} = 6.45$, see Fig. 3, and the flux obtained from a quasi-one-dimensional flow calculation (for a pressure ratio of 2.6), using Eq. (1), i.e., $(m)_{qs} = 11.87$. This results in a discharge coefficient of $\zeta = (m)_{\max}/(m)_{qs} = 0.54$. This value agrees very well with the empirically obtained discharge coefficient of $\zeta = 0.55$ obtained for the same perforation ratio (Onodera and Takayama 1990b).

The value of the discharge coefficient decreases as the main flow velocity decreases. In a former study, the experimentally obtained discharge coefficient varied from 0.35 to 0.2, whereas the Mach number decreased from 5.0 to 1.5 (Honda et al. 1974). Normally, the quasi-one-dimensional analysis deals with a choked flow at places where the critical pressure is reached. However, in reality the flow is not choked at places where the calculated values reaches the critical pressure due to unsteadiness of the flow field (Onodera and Takayama 1994). Therefore, for Mach numbers around and over the critical pressure values, the discharge coefficient decreases so as to match the empirically obtained value while using the quasi-one-dimensional flow model.

The present result of $\zeta = 0.54$ was obtained for the case where the perforation ratio is 0.4 and the incident shock wave Mach number is 1.54. However, from an engineering point of view, when a flow discharges through an orifice perpendicular to the main flow, a constant discharge coefficient of 0.54 should be used since ζ is practically insensitive to Ms (at least for the range of $1.5 \leqslant Ms \leqslant 5$).

5
Curvature of the diffracting shock wave

No reflected shock wave is observed from the perforated wall even when the incident shock wave collides obliquely with it (see Fig. 1a and b). A schematic illustration of this flow field is given in Fig. 4. When the frame of reference is attached to point P, which is the intersection of the incident shock wave with the perforated wall and the starting point of the boundary layer, then the boundary layer displacement thickness will increase quickly and become thicker than that developed over a flat plate under similar conditions. The reason for this fast increase in width is the existence of a flow discharge through the perforations (Schlichting 1968). The boundary layer is defined as the region where the velocity of the main flow component decreases owing to flow suction through the perforations. Therefore, the incident shock wave is temporarily perpendicular to the boundary layer edge. As a result, the incident shock wave encounters this "effective wall", and no wave reflection is observed.

Computational results for velocity vectors and isopycnics are shown in Fig. 5. Except for the limited bottom area of the incident shock wave, where the disturbed flow influences the wave, the flow field is quite uniform. Figure 6 shows the flow angle immediately behind the incident shock wave measured relative to the y-direction, so that 90° denotes the stream line perpendicular to the incident shock wave, and $y/\Delta y = 120$ stands for point P on the perforated wall surface, while y and Δy denote the distance in the y-direction and the interval of one computational mesh in the y-direction, respectively.

A streamline outside of the boundary layer, but close to its edge, must be parallel to the boundary layer edge, and the incident shock wave must be perpendicular to this streamline. This is valid only in the vicinity of point P. However as is evident from Fig. 6, the streamlines and the diffracted, curved, incident shock wave are almost perpendicular to each other for $y/\Delta y > 140$. On the other hand for y/Δ, $y < 140$ the flow angles between streamlines and the incident shock wave are smaller than 90°. Therefore, even at the region where the shock wave is inclined backward, except for the bottom where the wave front

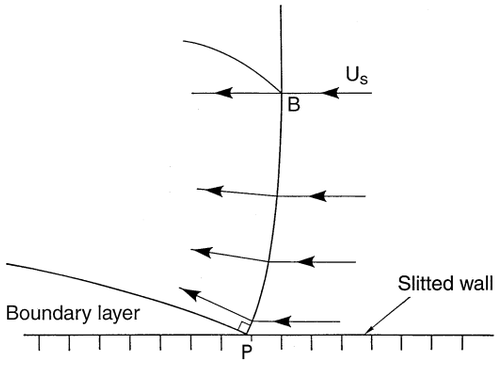

Fig. 4. Schematic of the considered flow field (shock fixed coordinate)

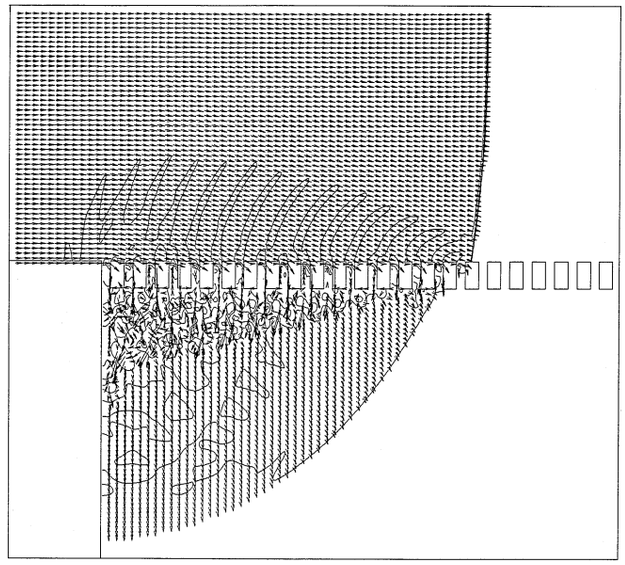

Fig. 5. Flow vectors and isopycnics in the investigated flow field

is strongly influenced by non-uniformity of the flow, the incident shock wave locally satisfies the normal shock relations.

Skews (1967) and Bazhenova et al. (1979) empirically showed the self-similarity pattern of shock wave diffraction around a corner. Similarly to their experiments, in the present case expansion waves from perforations continuously affect the wave front. Based on experimental results obtained for incident shock waves propagating at different Mach numbers it is apparent that the shape of the incident shock wave is self-similar, starting from the moment just after it hits the first slit. This self-similarity holds for a long time. This reaffirms the statement made earlier, namely that the flow disturbances generated along the perforated wall do not affect the shape of the incident shock wave. Even when and if disturbances catch-up with the incident shock wave, their effect in altering the shock wave shape (geometry) is negligibly small, less than 1% as was mentioned in the previous section (Onodera 1991). Therefore, the self-similarity is still valid. This result is probably caused by the relatively fine structure of the perforation, i.e. a relatively low value for the ratio of perforation periodicity and wall length. When the slit opening is made significantly wider, the resulting wave pattern will be different because disturbances emanating from each perforation will have a stronger effect on the considered flow field.

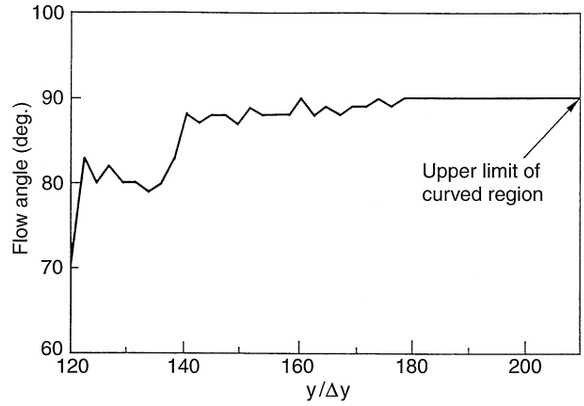

Fig. 6. Flow direction just behind the incident shock wave

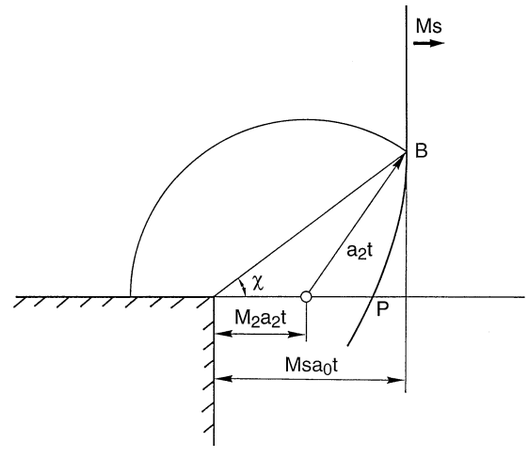

Fig. 7. Diffraction of shock wave around the corner

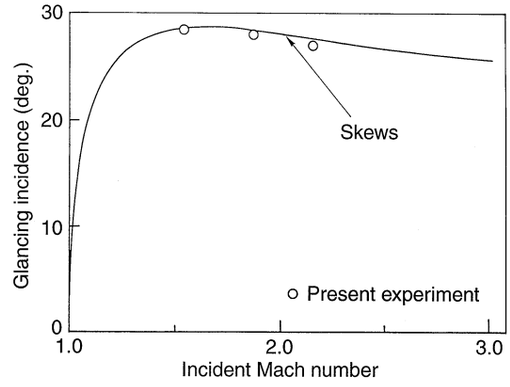

Fig. 8. The glancing incidence angle vs. *Ms*

The curved region of the incident shock wave terminates at the point where the expansion wave, emerging from the first

slit, catches up with the incident shock wave. The place at which a curvature in the incident shock wave is first noticed was defined in terms of the angle χ (glancing incidence, see Fig. 7). Based on geometrical relations Skews (1967) suggested the following expression for χ;

$$\chi = \arctan \frac{(Ms^2-1)((\gamma-1)Ms^2+2)}{(\gamma+1)Ms^4} \qquad (2)$$

In the present case, the angle between the straight line connecting this limit to the first slit and the perforated wall corresponds to the glancing incidence χ. In Fig. 8, the present experimental results are compared with those obtained while using Eq. (2). It is apparent that good agreement exists between the two.

In Fig. 9 the dependency of the downward velocity component (expressed in a non-dimensional form, i.e., as M_4),

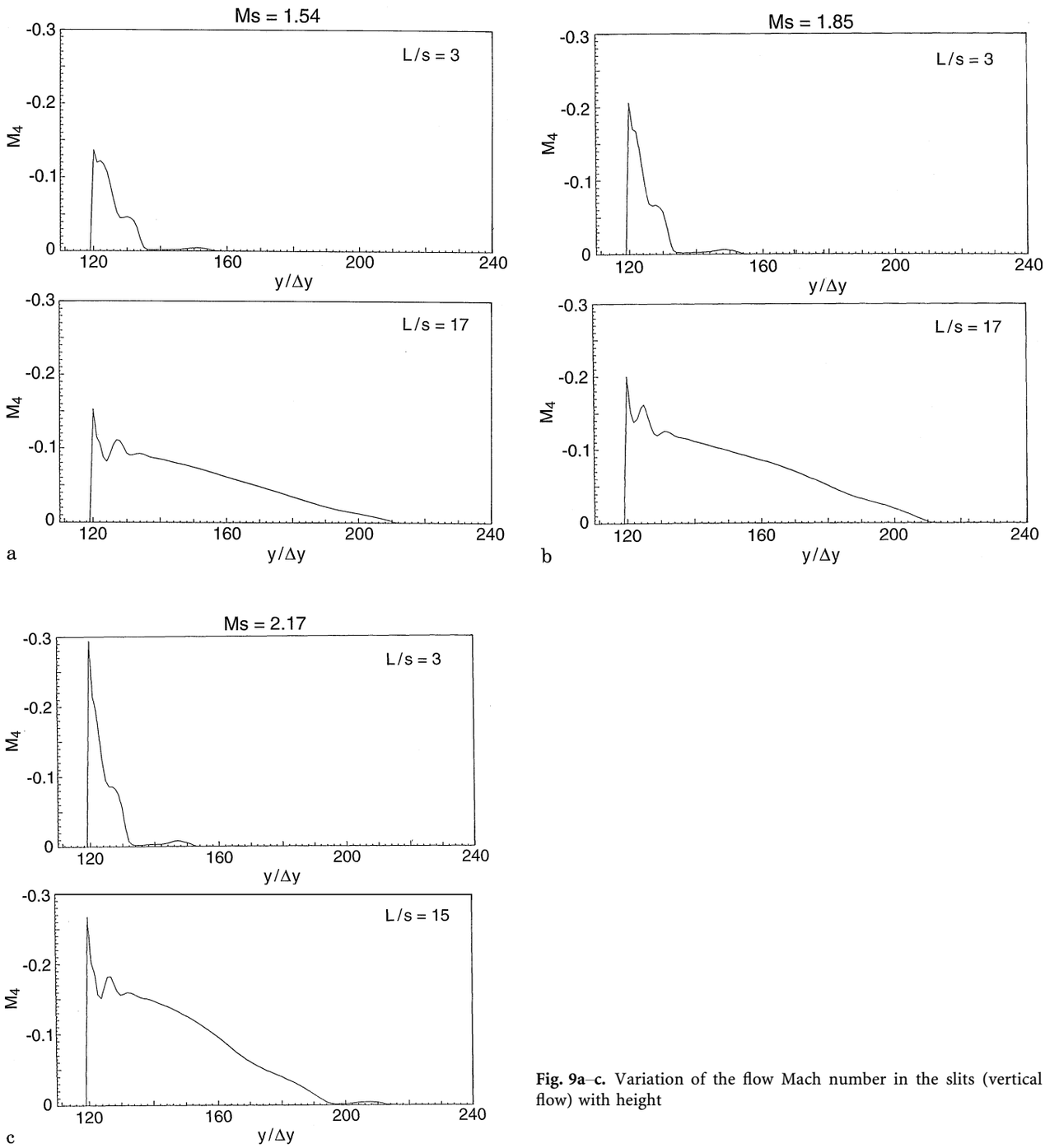

Fig. 9a–c. Variation of the flow Mach number in the slits (vertical flow) with height

just behind the incident shock wave, on distance (measured along the y-axis) is shown. The value of the vertical velocity component was averaged over the perforation width. Except of a region in close proximity to the perforated wall ($y/\Delta y = 120$), M_4 decreases smoothly until it reduces to zero at a certain height corresponding to the glancing incidence χ, for a given Ms.

The upper limit of the region where the flow is strongly disturbed behind the incident shock wave corresponds to the area influenced by the expansion wave, which emerges from the second perforation behind the incident shock wave. Therefore, the strongly disturbed region is confined to a limited area behind the incident shock wave. The shape of the curved incident shock wave is nearly self-similar when it propagates over uniformly distributed perforations.

If the velocity distribution between point P and point B (upper limit of the curved region of the incident shock wave) in Fig. 7 is a function of height only, i.e., $v_4 = a_4 M_4 \equiv f(y)$ where a_4 denotes the speed of sound inside the perforation, and the influence of the mass out-flow through the perforations on the main flow is negligibly small, then the streamlines inclination angle just behind the shock wave is given by

$$\theta = \arctan(\zeta\, \varepsilon\, \rho_4 v_4 / \rho_2 u_2), \tag{3}$$

where ρ is density. Assuming that $\rho_2 = \rho_4$ then,

$$\theta = \arctan(\zeta\, \varepsilon\, f(y)/u_2), \tag{4}$$

where $f(y)$ is a function of height y only. As can be seen from Fig. 6, the streamlines are almost perpendicular to the curved incident shock wave. Therefore, when θ is determined from Eq. (4), the inclination of the incident shock wave is expressed as $(90 - \theta)$ degree for a given height y. Consequently, since θ is the angle with which the incident shock wave inclines locally at a given height, the shape of the incident shock wave is obtained as an envelope to these tangents, and at point B it becomes zero.

Approximating the downward flow velocity distribution shown in Fig. 9 by a quadratic function and inserting this expression into Eq. (4) provides the shape of the incident shock wave. An example is shown, along with numerical results, in Fig. 10.

The obtained approximated shape of the shock wave is compared with experimental results in Fig. 11. In this figure the results are presented in a dimensional form, not normalized like a Whitham (1957). This presentation was chosen in order to ease detecting the influence of the disturbed region at the foot of the shock wave. Good agreement was found between the two, except for an area in close proximity to the perforated wall where flow non-uniformity caused by perforations strongly influences the shape of the shock wave.

Consequently, once the discharge coefficient of a perforated wall is determined, actual shock wave properties can be deduced easily. This could be very helpful in many engineering applications.

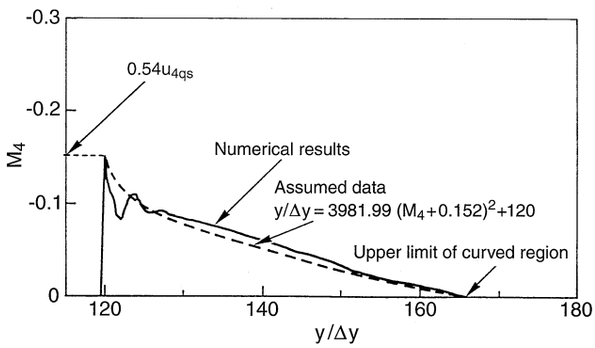

Fig. 10. Comparison between approximated downward velocity and computation results

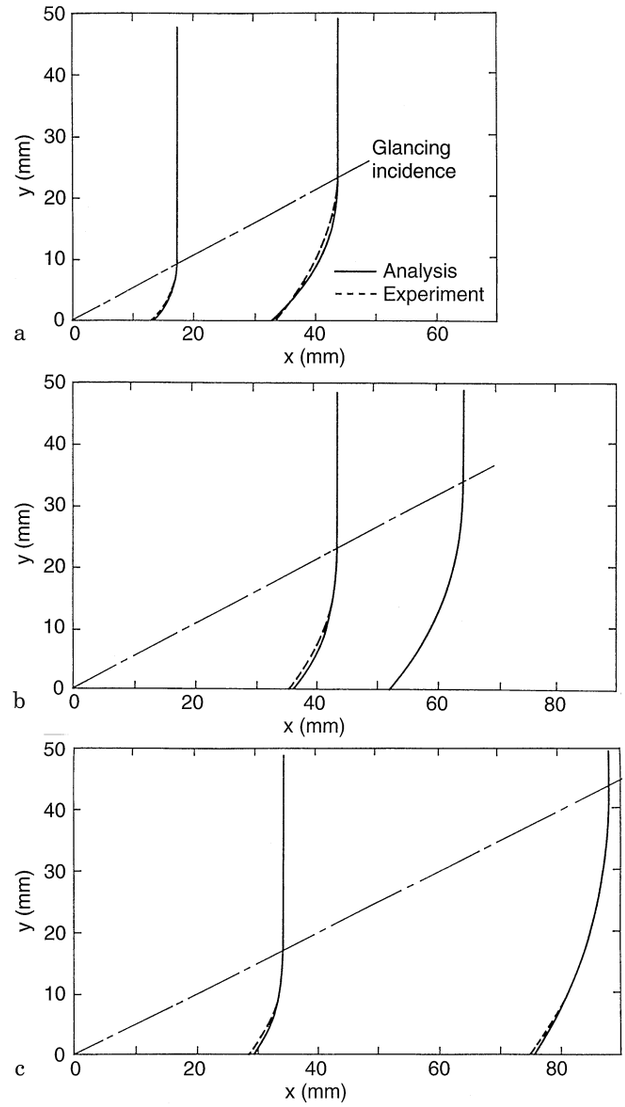

Fig. 11a–c. Comparison between analytical and experimental shock wave shapes. **a** $Ms = 1.54$; **b** $Ms = 1.85$; **c** $Ms = 2.15$

6 Summary of results

Shock wave propagation over a perforated wall was studied by means of optical flow visualization and numerical simulation

using a TVD scheme. The results were compared with a quasi-one-dimensional flow analysis. By incorporating the numerically obtained discharge coefficient (and using the static pressure behind the incident shock wave instead of the stagnation pressure as the effective reservoir condition) into a quasi-one-dimensional analysis, the shape of incident shock wave was predicted. The obtained results can be summarized as follows:

(1) The results obtained from a TVD numerical analysis agree very well with interferometric findings.

(2) A discharge coefficient of 0.54 was obtained by comparing the quasi-one-dimensional analysis with numerical results. This value agrees well with the experimentally obtained values. From an engineering point of view this value can be applied to a wide range of incident shock wave Mach numbers.

(3) The flow direction just behind the curved incident shock wave is almost perpendicular to the shock wave front, except for the strongly disturbed region at the foot of the incident shock wave.

(4) The shape of the curved incident shock wave, which inclined backward, was well predicted by employing the above mentioned discharge coefficient in the analysis.

References

Aoki T; Kashimura H; Nonaka Y; Matsuo K (1991) Discharge of a compression wave from an open end of a tube. Proc 18th Int Symp Shock Waves, Sendai, 1331–1334

Bazhenova TV; Gvozdeva LG; Zhilin Yu V (1979) Change in the shape of the diffracting shock wave at a convex corner. Acta Astronautica 6: 401–412

De Bore PCT (1963) Curvature of shock fronts in shock tubes. Phys Fluids 6: 962–971

Deckker BEL; Koyama H (1983) Motion of a weak shock wave in a porous tube. Proc 14th Int Symp Shock Tube and Waves, Sydney, 239–246

Frolov SM; Gelfand BE (1991) Shock wave attenuation in channels with perforated walls. Proc 18th Int Symp Shock Waves, Sendai, 197–202

Honda M; Takayama K; Onodera O (1974) Shock wave propagation along a perforated tube (in Japanese). Mem Inst High Speed Mech, Tohoku Univ 34: 1–27

Kage K; Kawagoe S; Matsuo K (1992) Numerical study of compression waves produced by high-speed trains entering a tunnel (in Japanese). Trans Jpn Soc Mech Eng 50-457B: 2094–2103

Lee LHS; Ostrowski PP; Wu JHT (1976) Shock attenuation by a single transverse slit. J Fluid Mech 76: 675–688

Matsumura S; Onodera O (1991) Noise induced by weak shock waves in automobile exhaust systems. Proc 18th Int Symp Shock Waves, Sendai, 1327–1330

Okutsu R (1984) Generation of noise or vibration related to high pressure reducing or control (in Japanese). Trans Jpn Soc Mech Eng 50-457B: 2094–2103

Onodera H; Takayama K (1990a) Shock wave propagation over slitted wedges. Rep Inst Fluid Sci Tohoku Univ 1: 45–66

Onodera H; Takayama K (1990b) Interaction of a plane shock wave with slitted wedges. Exp Fluids 10: 109–115

Onodera H (1991) Shock wave propagation over perforated media (in Japanese). PhD Theses, Tohoku Univ

Onodera H; Takayama K (1994) An analysis of shock wave propagation over perforated wall and its discharge coefficient. JSME Int J Ser B, 37: 497–502

Schlichting H (1968) Boundary layer theory, 6th ed. McGraw-Hill, New York, 367–383

Skews BW (1967) The shape of a diffracting shock wave. J Fluid Mech, 29: 297–304

Szumowski AP (1971) Attenuation of a weak shock wave in a porous tube. Shock Tube Research 14. Chapmann & Hall, London, 1–10

Whitham JB (1957) A new approach to problems of shock dynamics. J Fluid Mech 2: 145–171

Yee HC (1989) A class of high-resolution explicit and implicit shock-capturing methods. NASA Tech Mem 101088